ELECTRONIC SUPPORTING INFORMATION

Reactive Mode Composition Factor Analysis of Transition States: The Case of Coupled Electron-Proton Transfers

Mauricio Maldonado-Domínguez,[a] *Daniel Bím,*[a,b] *Radek Fučík,*[c] *Roman Čurík*[a]
and Martin Srnec[a,]*

[a]J. Heyrovský Institute of Physical Chemistry, The Czech Academy of Sciences, Dolejškova 3, Prague 8, 18223, Czech Republic.

[b]Institute of Organic Chemistry and Biochemistry, Czech Academy of Sciences, Prague 6, 16610, Czech Republic

[c]Department of Mathematics, FNSPE CTU, Prague

Corresponding Author

*E-mail: martin.srnec@jh-inst.cas.cz

Supporting Information Contents

Computational Details

All reactant, transition state and product (R, TS, P) geometries were optimized using the Gaussian09 program at the B3LYP+D3/def2-TZVP/CPCM level of theory.[1] Free energy changes, ΔG, were evaluated from equilibrium geometries using equation (S1):

$$\Delta G = \Delta E_{\mathrm{el}} + \Delta G_{\mathrm{solv}} + \Delta\ [E_{ZPVE} + pV - RT\ \ln Q] \tag{S1}$$

where gas-phase ΔE_{el} and $\Delta[E_{ZPVE} + pV - RT \ln Q]$ terms were obtained at the same level of theory as the optimized structures, while ΔG_{solv} was calculated using the COSMO-RS approach with radii-based isosurface cavity, ($cosmo_isorad keyword) and the COSMOtherm parameter set BP_TZVPD_FINE_C30_1501.ctd as available in COSMOtherm15.[2] The COSMO-RS calculations were carried following the recommended protocol: the BP86/def2-TZVPD/COSMO($\varepsilon_r = \infty$) ≡ $E_{\mathrm{COSMO},\infty}$ and BP86/def2-TZVPD/*in vacuo* ≡ $E_{\mathrm{in\ vacuo}}$ single-point calculations are used to calculate $G_{solv}(T) = (E_{\mathrm{COSMO},\infty} - E_{\mathrm{in\ vacuo}}) + \mu_{\mathrm{COSMO\text{-}RS}}(\mathrm{T})$, where $\mu(\mathrm{T})$ is the temperature-dependent COSMO-RS chemical potential as defined in ref 3. Intrinsic reaction coordinate (IRC) calculations were performed to connect all TS with the corresponding R and P structures.

All activation free energies, $\Delta G^{\neq}$ were taken as the difference between the free energy of the TS in the S = 2 state (G_{TS}) and $G_{\mathrm{Sub}} + G_{\mathrm{R}}$ + 1.9 kcal mol^{-1}, where G_{Sub} is the free energy of a singlet substrate and G_{R} is the free energy of a ferryl complex in its ground spin state (S = 1 or S = 2). A value of 1.9Δn kcal mol^{-1} has been applied to correct the computed values to the 1 mol L^{-1} standard state (a value of 1.9 kcal mol^{-1} corresponds to the conversion of a 1 bar standard state in the gas phase to 1 mol L^{-1} concentration in solution at 298K; Δn is the change in the number of moles).[4]

All reaction free energies ΔG_0, were considered as the difference between the free energy of the isolated reactants and products, $\Delta G_0 = (G_{\mathrm{Rad}} + G_{\mathrm{P}}) - (G_{\mathrm{Sub}} + G_{\mathrm{R}})$, where G_{Rad} is the free energy of a doublet product radical and G_{P} is the free energy of a ferric hydroxide complex in its ground spin state (S = 5/2).

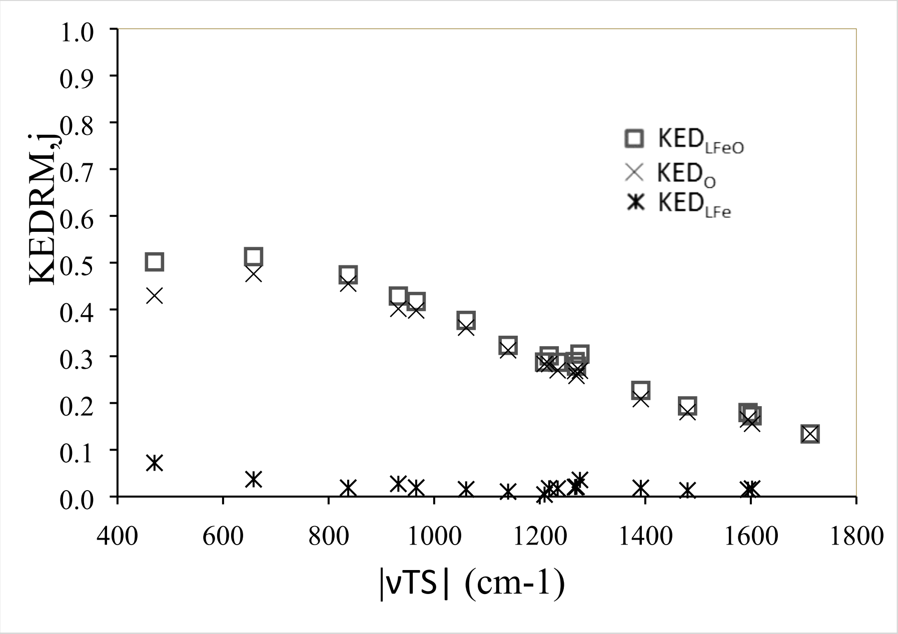

Figure S1. Reactive mode composition of the LFeO fragment across the set of reactions. As observed, most of the motion in this fragment is located on the oxygen atom.

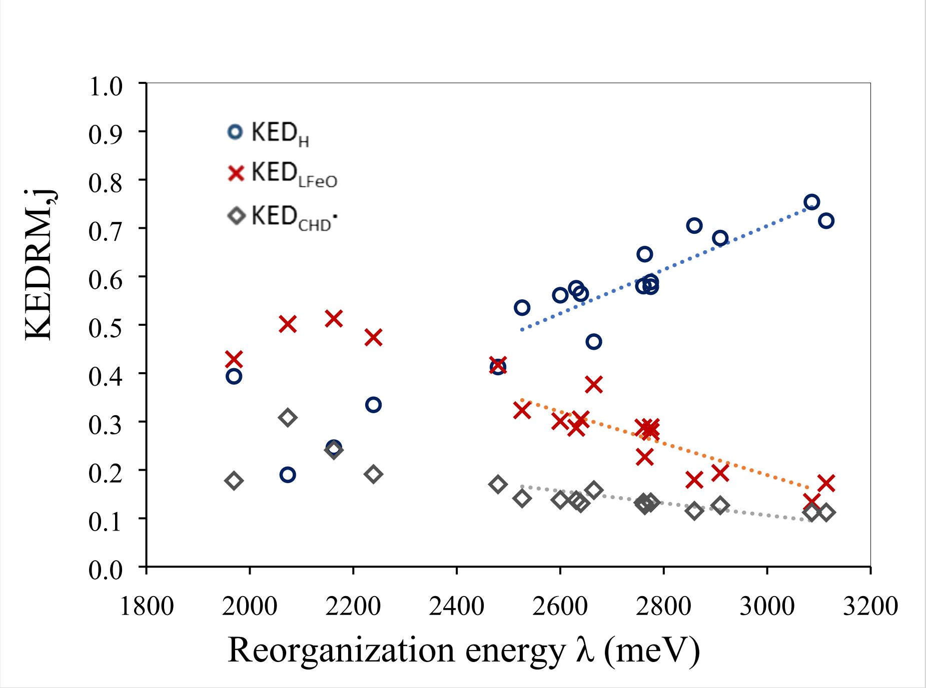

Figure S2. Evolution of KED$_{RM,j}$ with Marcus reorganization energy

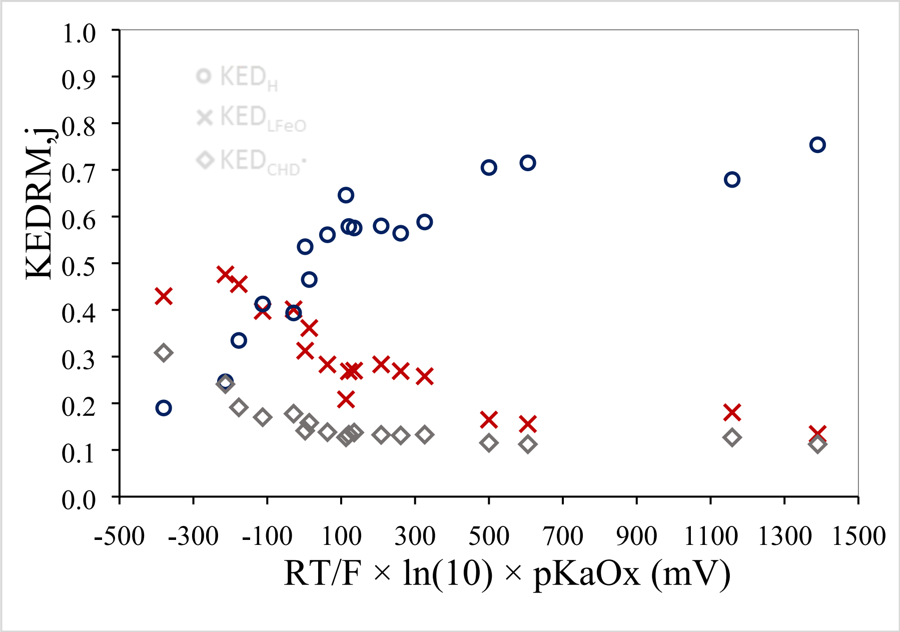

Figure S3. Evolution of KED$_{RM,j}$ with the pKa of the Fe^{IV}O complex.

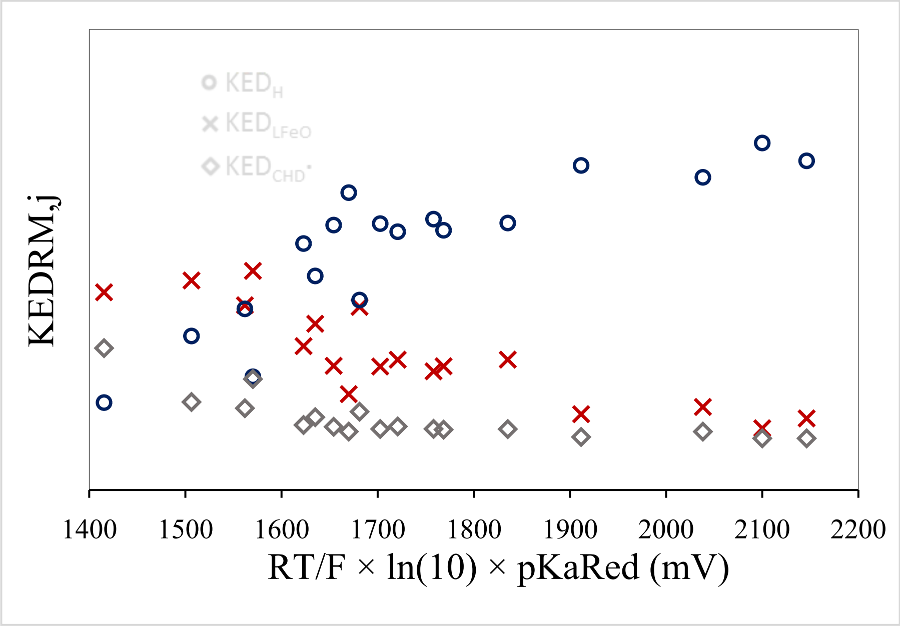

Figure S4. Evolution of KED$_{RM,j}$ with the pKa of the Fe^{III}O complex.

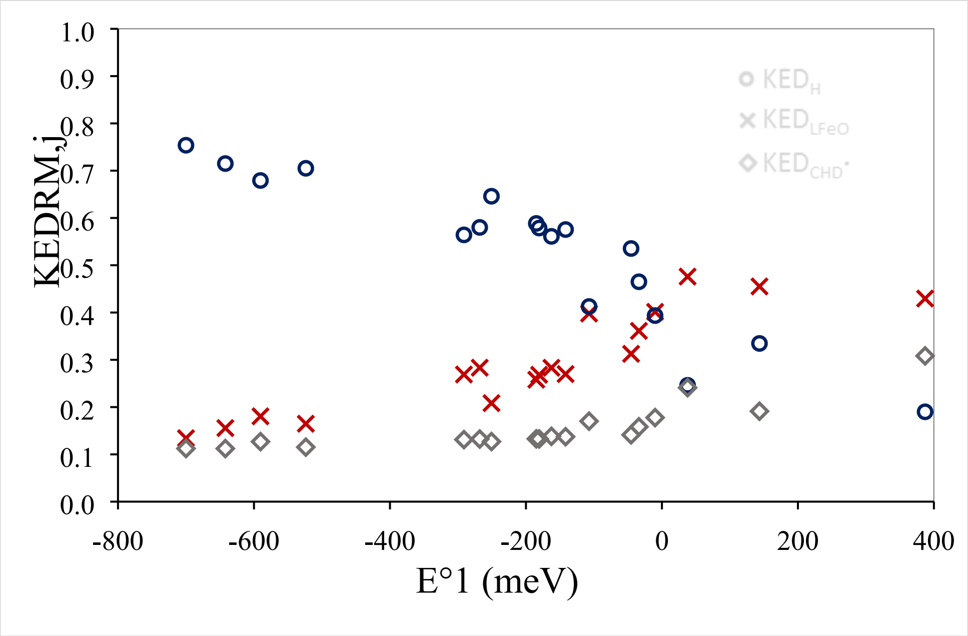

Figure S5. Evolution of $KED_{RM,j}$ with the reduction potential E° of the $Fe^{IV}O$ complex.

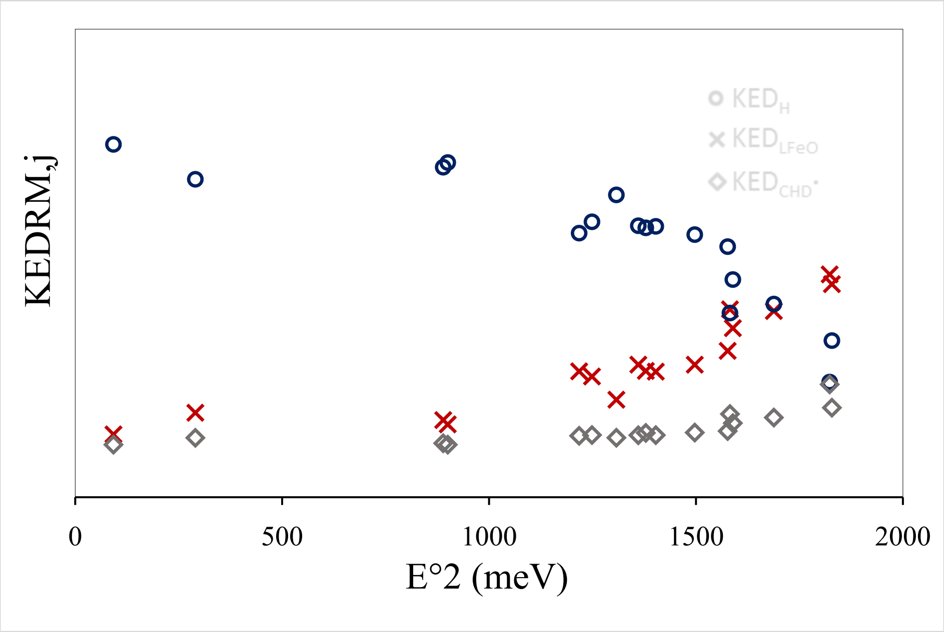

Figure S6. Evolution of $KED_{RM,j}$ with the reduction potential E° of the $Fe^{IV}OH$ complex.

Appendix S1: RMCF analysis of $[Fe^{IV}O(TQA)(Cl^{-})]^{+}$ derivatives

To test the general applicability of the RMCF analysis, we pursued the CPET reactivity of a second series of oxidants with cyclohexane as substrate, based on the $[Fe^{IV}O(TQA)(Cl^{-})]^{+}$ scaffold[5] and a set of derivatives (Scheme S1). This complex is activates the strong C-H bond in cyclohexane despite having a low driving force for CPET, thus being an interesting subject for our RMCF analysis.

Scheme S1. $[Fe^{IV}O(TQA)(Cl^{-})]^{+}$ scaffold and derivatives studied using the RMCF methodology on their CPET reactivity with cyclohexane as a substrate.

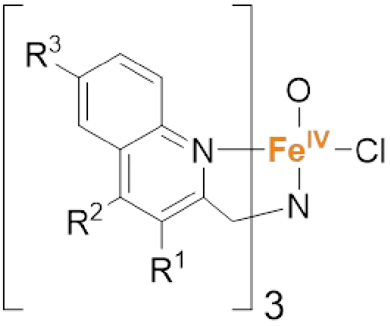

	R¹	**R²**	**R³**
1	H	H	H
2	CN	H	H
3	H	CN	H
4	CN	CN	H
5	NO_2	H	H
6	H	NO_2	H
7	OMe	H	H
8	NMe_2	H	H
9	H	NMe_2	H
10	NMe_2	H	NMe_2

The results show that this reactivity is assisted by a large asynchronicity in favour of electron transfer which is reflected in the reactive mode composition factor (Figure S7A) and the Gibbs energy of activation (Figure S7B), which smoothly evolves along the corresponding set of reactions. These additional results allowed us to further illustrate how KED evolves as a function of asynchronicity and how this translates into differential atomic motion at the CPET transition state which reflects on the magnitude of $\Delta G^{\neq}$.

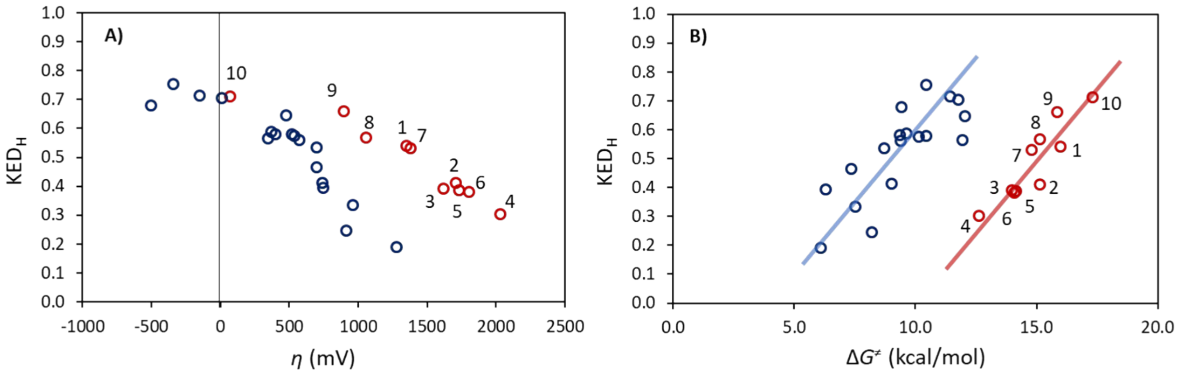

Figure S7. A) Evolution of $\mathrm{KED_H}$ in the series of CPET reactions between $[\mathrm{Fe^{IV}O(TQA)(Cl^-)}]^+$ -derived oxidants (numbered red circles) and cyclohexane, as a function the asynchronicity factor η, and B) changes in $\Delta G^{\neq}$ associated with the redistribution of $\mathrm{KED_H}$ at the reactive mode. The TMC series, discussed in the main text, is included in both plots for comparison as blue unlabelled circles.

Appendix S2: Calculation of tunneling corrections

The tunneling correction to the free energy activation barrier at each temperature was calculated according to the Eckart method, using our home-built program KAPPA. Calculation of a transmission coefficient $\kappa = \kappa(\beta)$ with $\beta = 1/(k_B T)$ was implemented in analogy to the TheRate program; i.e., Eq. (12) in ref. 6:

$$\kappa(\beta) = \frac{\int_{0}^{+\infty} P(E) e^{-\beta E} dE}{\int_{E_*(T)}^{+\infty} e^{-\beta E} dE}, \tag{S10}$$

where

$$P(E) = \begin{cases} 0, & E \in (0, E_1) \\ p(E), & E \in [E_1, E_*) \\ 1 - p(2E_* - E), & E \in [E_*, 2E_* - E_0) \\ 1, & E \in [2E_* - E_1, +\infty) \end{cases}$$

where (S11)

$$p(E) = \frac{1}{1 + exp(2\theta(E))}, \tag{S12}$$

where

$$\theta(E) = \frac{2\pi}{h}\sqrt{2\mu_{eff}} \int_{S_l}^{S_r} \sqrt{V_d(s) - E}\, ds, \tag{S13}$$

where

$$V_d(y) = \frac{ay}{1+y} + \frac{by}{(1+y)^2} + c, \tag{S14}$$

where

$$y = y(s) = y^{\alpha(s - s_0)},\tag{S15}$$

where

s_l and s_r together with $y_l = y(s_l)$ and $y_r = y(s_r)$ satisfy:

$$V_d(y_l) = V_d(y_r) = E\tag{S16}$$

Eq. (S16) is a quadratic equation that can be written in the form:

$$Ay^2 + By + C = 0,\tag{S17}$$

where

$$A = E - c - a,\tag{S18}$$

$$B = 2(E - c) - b - a,\tag{S19}$$

$$C = E - c,\tag{S20}$$

where $A > 0$ is assumed.

If $D = B^2 - 4AC > 0$, then Eq. (S17) has two real roots:

$$y_l(E) = \frac{-B - \sqrt{D}}{2A},\tag{S21}$$

$$y_r(E) = \frac{-B + \sqrt{D}}{2A},\tag{S22}$$

such that $y_l < y_r$. For the case $D = 0$, Eq. (S17) has a single root for which V_d is maximal. This root is denoted by E_* and from $D = 0$, we can express the root as:

$$E_* = c + \frac{1}{b}\left(\frac{a + b}{2}\right)^2.\tag{S23}$$

By virtue of Eq. (S15), the integral in Eq. (S13) can be transformed into the integration variable *y* as:

$$\theta(E) = \frac{2\pi}{h}\sqrt{2\mu_{eff}}\int_{y_l}^{y_r} \frac{1}{\alpha y}\sqrt{\frac{ay}{1+y} + \frac{by}{(1+y)^2} + c - E}dy \quad . \tag{S24}$$

In both integrals in Eqs. (S13) and (S24), we assume $E - c \geq 0$.

The integral in Eq. (S24) can be evaluated analytically as:

$$\theta(E) = \frac{2\pi^2}{\alpha h}\sqrt{2\mu_{eff}}[\sqrt{b} - \sqrt{E-c} - \sqrt{E-a-c}] \quad . \tag{S25}$$

Finally, the definition of *P* in Eq. (S11) allows to rewrite the integral in Eq. (S10) in a compact form as:

$$\kappa(\beta) = 1 + 2\beta\int_{E_1}^{E_*} P(E)sinh[\beta(E_* - E)]dE \quad . \tag{S26}$$

The evaluation of an integral in Eq. (S26) requires input of the following parameters:

i) *T*, temperature,

ii) μ_{eff}, reduced mass of the transition mode,

iii) α, range coefficient; $\alpha = \sqrt{-\frac{\mu_{eff}(\omega^{\neq})^2 B}{2V^{\neq}(V^{\neq} - A)}}$,

where

$V^{\neq}$ is the classical barrier height,

$\omega^{\neq}$ is the imaginary frequency,

A is the classical potential energy of reaction (from RC to PC), and

$B = (2V^{\neq} - A) + 2\sqrt{V^{\neq}(V^{\neq} - A)}$.

iv) a, zero-point corrected energy of reaction (from RC to PC)

v) b, zero-point corrected B; $b = \left(2V^{\neq G} - a\right) + 2\sqrt{V^{\neq G}(V^{\neq G} - a)}$, where $V^{\neq G}$ is the zero-point energy corrected barrier height

vi) c, sum of the zero-point energies of the two reactants (set to zero)

Appendix S3: Defining TS symmetry based on KED

In the main text, the TS (a)symmetry, pointed out by Westheimer during his analysis of kinetic isotope effects on H-transfer reactions,[7] is reinterpreted by measuring the TS location based solely on $\mathrm{KED_H}$. An alternative and straightforward measure of (a)symmetry would be the difference in KED between the fragments flanking the transferred H-atom, namely the nascent radical and the iron-oxo unit plus its ligands: $\mathrm{KED_{LFeO}}$ - $\mathrm{KED_{Subs}}$. One can easily reckon that as the difference approaches zero, the symmetry would be maximal. The highest asymmetry should then correspond to scenarios where it tends towards either 1 or -1.

This formulation provides an intuitive picture of the redistribution of kinetic energy at the reactive mode and its influence on KIE. It is illustrative to look at the evolution of KIE with KED asymmetry as defined in the previous paragraph within the set of 18 reactions studied in this work, before and after applying Eckart tunneling corrections:

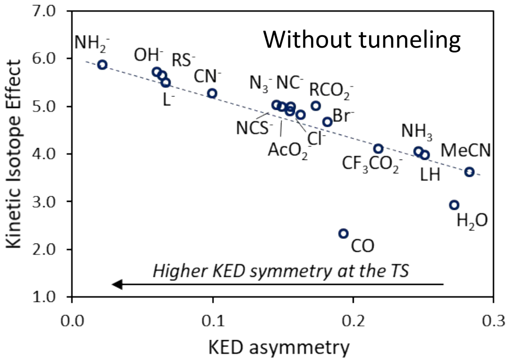

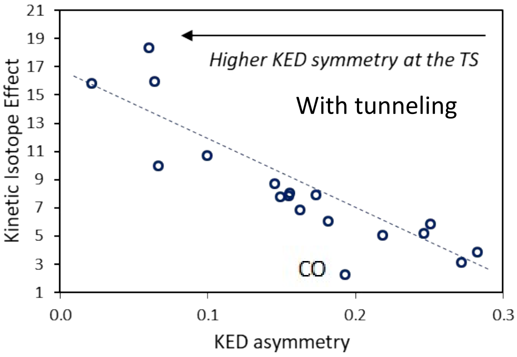

The evolution of the uncorrected KIE with KED asymmetry is remarkably linear. When tunneling corrections are included the trend preserves, albeit scattered. It is also noticeable that an outlier exists, with CO as axial ligand. We apply the RMCF analysis to understand this in Appendix S3.

We foresee a possible pitfall to this alternative description of the TS based on KED asymmetry. When comparing transition states, one can imagine two structures with different $\mathrm{KED_H}$ but nearly identical KED asymmetry, as exemplified in the following hypothetical reactions:

Reaction 1: A---H---B ($KED_H = 0.70$, $KED_A = 0.12$, $KED_B = 0.18$)

Reaction 2: Y---H---Z ($KED_H = 0.50$, $KED_Y = 0.19$, $KED_Z = 0.31$)

In both cases, KED asymmetry is 0.12, which would misleadingly suggest reactive modes (hence, transition states) with the same character. In contrast, KED_H points towards an earlier TS for reaction 2, with presumably lower KIE and tunneling contributions than reaction 1.

Appendix S4: Using RMCF to analyze the character of the reactive mode

The reactive mode (or any real mode) can be readily compared with the full set of modes at TS by calculating the KED deviation between them. To measure the deviation of KED we compute the root mean square deviation between mode α and the reactive mode, RM:

$$RMSD_{\alpha,RM} = \sqrt{\frac{1}{n}\sum_{j}\left(KED_{j,\alpha} - KED_{j,RM}\right)^2} \tag{S27}$$

Since KED is a scalar quantity, no information related to directionality of motion is included in the analysis. Despite this apparent shortcoming, it proves insightful as illustrated with the analysis of the outlier in the plot where the axial ligand is CO (reproduced from Appendix S2, outlier shown as a red cross):

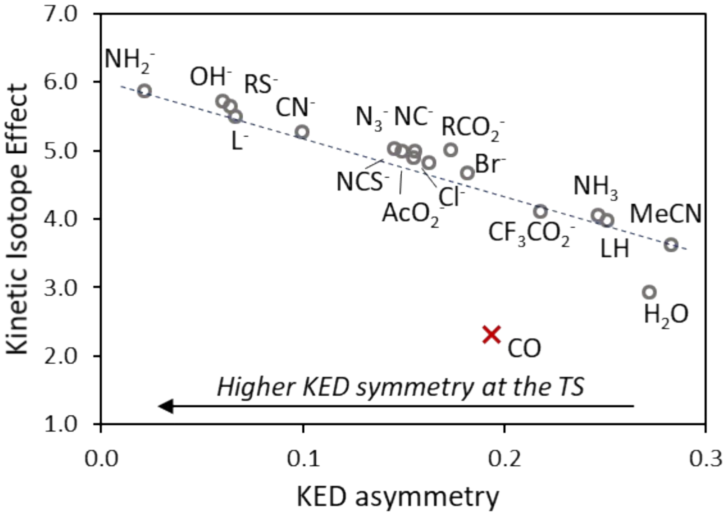

The histogram condensing the RMSD between the reactive mode and the full set of real modes for this system is the following:

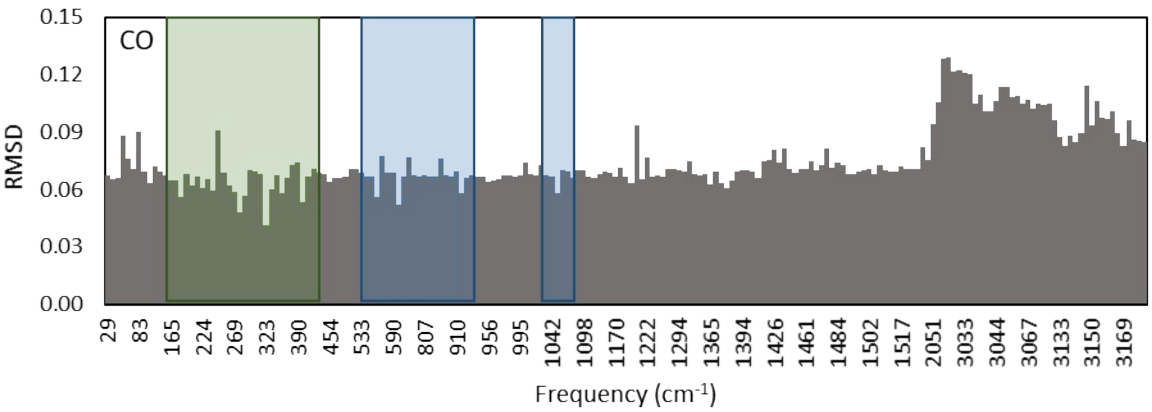

Some general features are (a) a relatively high RMSD values for the set of high-frequency C-H stretching modes (from ca. 2900 cm^{-1} onwards) and (b) a nearly constant RMSD value for the rest of the modes. We highlight the zones where the largest resemblance (low-RMSD) to the reactive mode appears. Inspection of these modes reveals that the CO-ligated complex, the earliest and most redox-driven within the set of reactions, exhibits a TS resembling rocking and wagging of the reactive CH_2 group (blue highlight) in the substrate but no noticeable C-H stretching. *Thus, H-motion is not only low ($KED_H = 0.19$), but the character of the reactive mode is substantially different to the rest of the set.* The reactive mode also involves ample FeO motion (blue-shaded region), as expected from the high $KED_{LFeO} = 0.50$. The RMCF analysis facilitates this rationalization and points out another pitfall of using KED asymmetry to predict relative kinetic isotope effects within sets of reactions: subtle mechanistic features can dramatically affect KED asymmetry whereas KED_H proved robust throughout the study.

Looking at some other reactive systems under the same lens clarifies the previous analysis:

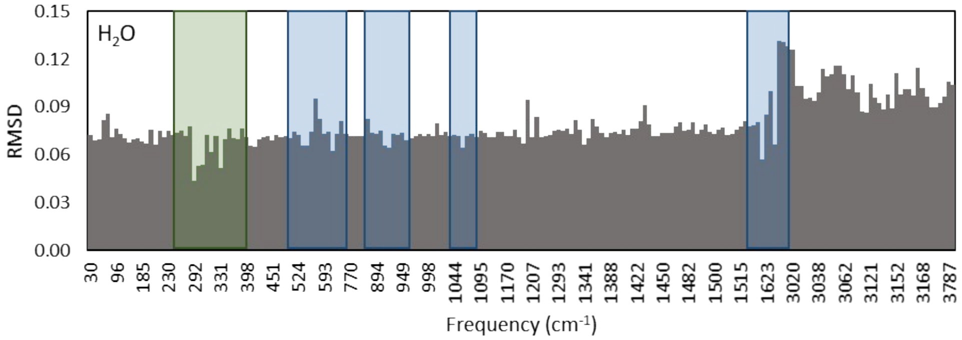

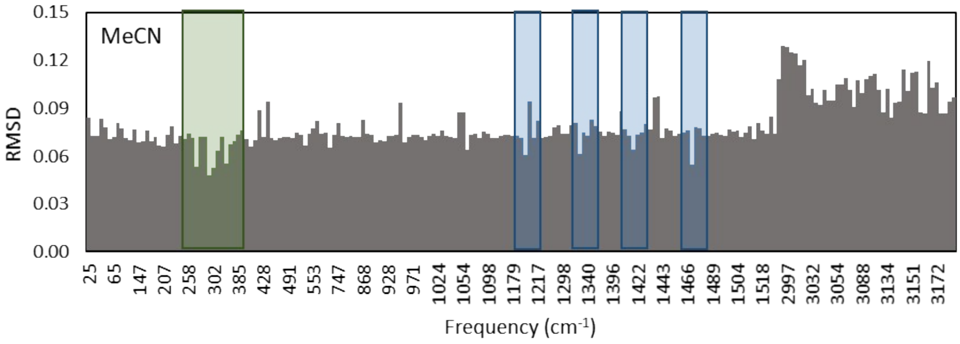

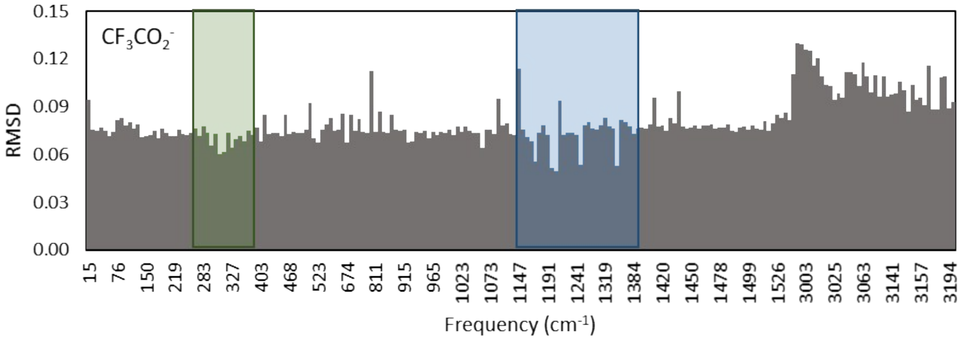

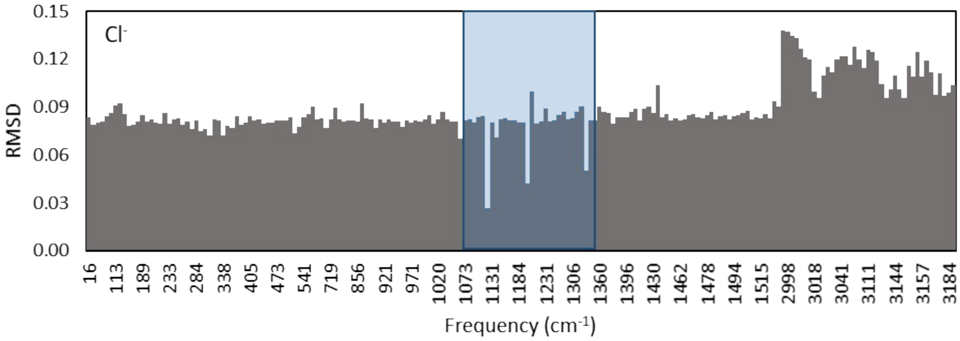

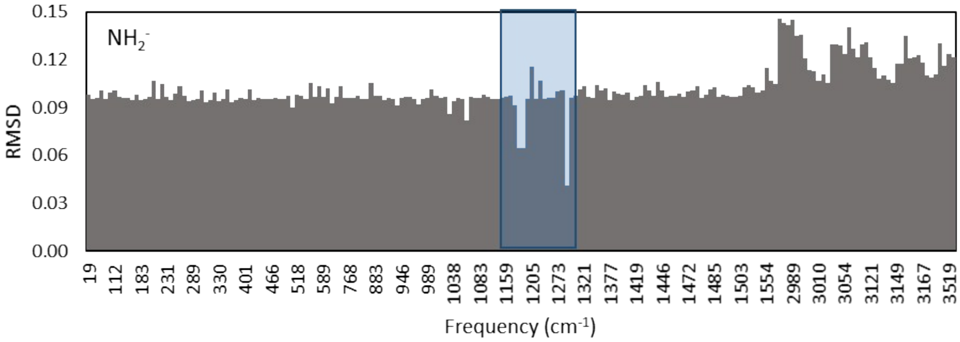

From H_2O-ligation onwards, C-H stretching motion (identified by low-RMSD modes in the medium-frequency range) plays an increasingly important role in the chemical step and, thus, the rest of the set behaves monotonically.

References

---

[1] a) V. Barone, M. Cossi, *J. Phys. Chem. A* **1998**, *102*, 1995-2001. b) M.Cossi, N. Rega, G. Scalmani, V. Barone, *J. Comput. Chem.* **2003**, *24*, 669.

[2] COSMOtherm 19, COSMOlogic GmbH & Co KG, http://www.cosmologic.de

[3] A. Klamt, *J. Phys. Chem.* **1995**, *99*, 2224.

[4] D. M. Camaioni, C. A. J. Schwerdtfeger, *Phys. Chem. A*, **2005**, *109*, 10795.

[5] M. Puri, A. N. Biswas, R. Fan, Y. Guo, L. Que Jr. *J. Am. Chem. Soc.* **2016**, *138*, 2484.

[6] W. T. Duncan, R. L. Bell, T. N. Truong, *J. Comput. Chem.* **1998**, *19*, 1039.

[7] F. H. Westheimer, *Chem. Rev.* **1961**, *61*, 265.